Direct observation of the perpendicular shape anisotropy and thermal stability of p-STT-MRAM nano-pillars

Trevor P. Almeida[1,2]*, Steven Lequeux[3], Alvaro Palomino[3], Ricardo C. Sousa[3], Olivier Fruchart[3], Ioan Lucian Prejbeanu[3], Bernard Dieny[3], Aurélien Masseboeuf[3] and David Cooper[1]

[1]Univ. Grenoble Alpes, CEA, Leti, F-38000 Grenoble, France.

[2]SUPA, School of Physics and Astronomy, University of Glasgow, G12 8QQ, UK.

[3]Univ. Grenoble Alpes, CEA, CNRS, Grenoble INP, SPINTEC, 38000 Grenoble, France.

Supplementary information

*Corresponding author:

Tel: +44 (0) 141 330 4712

Email: trevor.almeida@glasgow.ac.uk

This PDF file includes:

S1: Dipolar field calculation

We used Hubert's formalism[1] for calculating the magnetostatic field $\mathbf{H}_\mathrm{d}(\mathbf{r})$ arising from the pillar, also called demagnetizing field inside the pillar, and stray field outside the pillar. Estimating the magnetostatic field is crucial to extract magnetization $\mathbf{M}(\mathbf{r})$ from the experimental results, which pertain to the magnetic induction field $\mathbf{B} = \mu_0(\mathbf{H} + \mathbf{M})$.

Hubert's formalism relies on the so-called F_{ijk} functions, related to the i^{th}, j^{th} and k^{th} integrals along x, y and z, respectively, of the core function $V(\mathbf{r})=1/\mathbf{r}$, involved in the calculation of the magnetostatic potential.

In practice, this formalism requires the consideration of prisms, not cylinders. Hence, as an approximation we considered a prism with the same height and cross-section as the experimental pillar: square section with $a = b = 15.24$ nm such as $ab = \pi r^2$, and $c = 60$ nm (see Fig. S1a for a schematic of such prism). Magnetic quantities are calculated for a charged plate in the *(x,y)* plane, associated with magnetization along the axis of the pillar :

- The magnetic potential is calculated with the F_{110} function
- The vertical component of magnetic field $\mathbf{H}_{\mathrm{d,z}}$ is calculated with the $\mathrm{F}_{11\text{-}1}$ function
- The vertical component of magnetic field integrated along the beam (y) is calculated with the $\mathrm{F}_{12\text{-}1}$ function
- The vertical component of magnetic field, integrated along the beam and averaged over a strip of height Δz, is calculated with the F_{120} function. Note that this quantity is directly related to the magnetic potential, averaged along the beam direction y.

As not all expressions for the above F_{ijk} functions are mentioned in the book of Hubert and Schäfer[1], here is the full list:

$F_{000}(x,y,z) = \frac{1}{\sqrt{x^2+y^2+z^2}}$,

with $\phi(x,y,z) = \frac{Q}{4\pi} F_{000}(x,y,z)$ the magnetostatic potential associated with the magnetic charge Q.

$$F_{110}(x,y,z) = yL_x + xL_y - P_z$$

$$F_{11-1}(x,y,z) = -\frac{P_z}{z}$$

$$F_{12-1}(x,y,z) = -zL_x - \frac{y}{z}P_z$$

$$F_{120}(x,y,z) = xyL_y + \frac{1}{2}(v-w)L_x - yP_z - \frac{1}{2}xr$$

with the following functions: $u = x^2$, $v = y^2$, $w = z^2$, $r = \sqrt{x^2 + y^2 + z^2}$, $L_x = \mathrm{Atanh}(x/r)$, $P_x = x\ Atan\ (yz/xr)$, with $L_x = 0$ and $P_x = 0$ for $x = 0$ (and permutations for y and z).

In practice, we then performed the calculation of the y-integrated z component of the dipolar field, further averaged along a z slice (with height 15 nm) around a given z position, similar to the experimental average made on experimental extractions. This allows us to subtract the suitable value of magnetic field, part of the experimentally-measured induction from cross-sections such as in Fig. 2d of the main manuscript. This can be applied to the two procedures we implemented (*i.e.* using the phase slope or the tomographic method respectively - see next section) to estimate the real magnetization value. It is worth noticing that our estimation may be affected by two important parameters:

1) The magnitude of dipolar magnetic field is strongly dependant on the selected vertical position of the slice (see Fig. S1d). To extract the most suitable data from the electron holography images and to calculate reliable values of magnetization, we selected the maximum experimental values of integrated induction. However, such experimental measurements are influenced by angles of projection as they are only sensitive to the in-plane component of the magnetic induction, and the extracted values includes these negative contributions from the demagnetizing field. Hence we are limited to finding a local extremum of induction from a 2D projection of a 3D magnetic field and assume that our local maximum truly corresponds to the middle height of the pillar (and the minimum of dipolar field), keeping in mind that our measurement could be affected by a remaining angle in the experimental projection.
2) All values computed here are given in [M] for the dipolar field and [M].nm for the y-integrated dipolar field. The latter are converted to Tesla (T.nm) based on the assumption of spontaneous magnetization of 1.2 Tesla[2]. A more accurate estimation would require an iterative procedure to account for the new corrected approximation of the spontaneous magnetization to compute new values of the demagnetization field. However, for our estimation such iterations should only act at the mT level, below our experimental errors. That is, the computation given in the next section is given in T.nm, knowing that it remains an approximation.

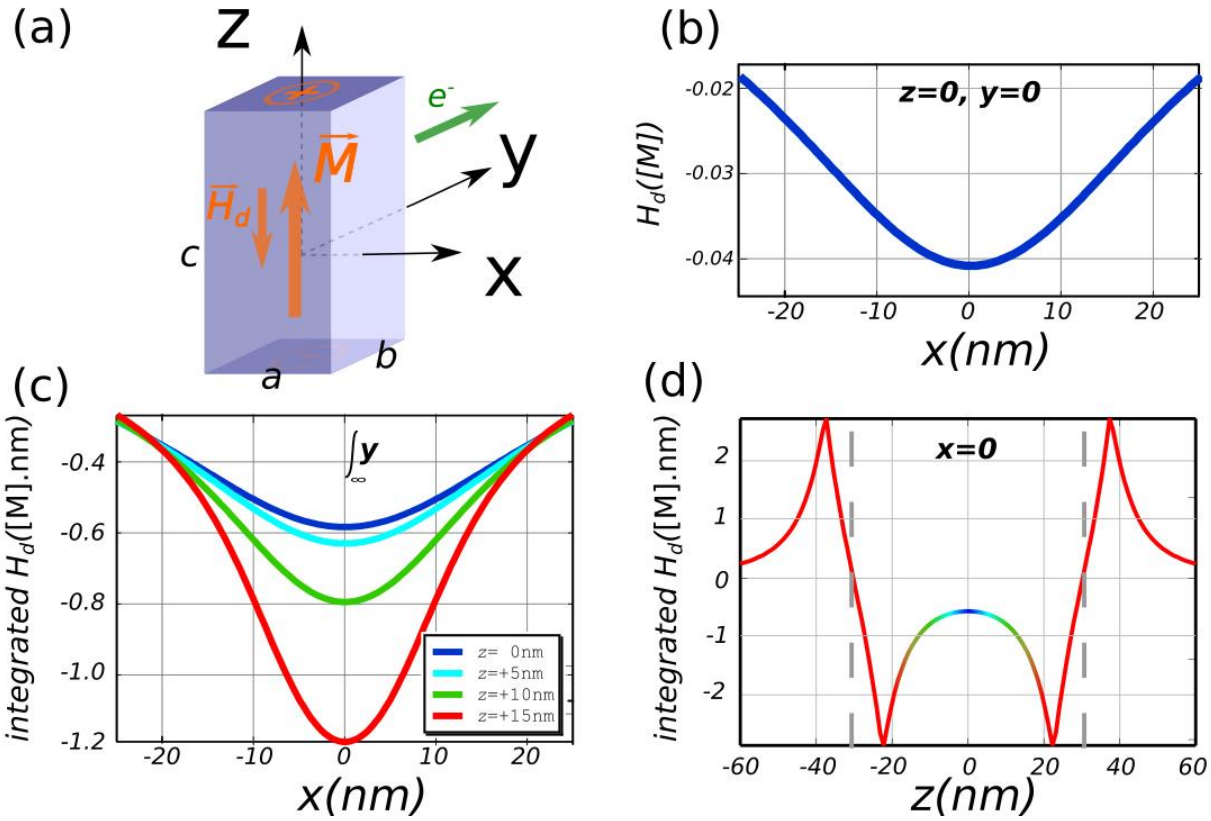

Figure S1 (a) Scheme of the prism used for the calculation with corresponding values given in the text. The origin of coordinates is at the center of the prism (b) x cross-section of the z component of the demagnetizing field at mid-height of the prism and y=0, further averaged along a z slice of height 15 nm to reproduce the experimental measurement. (c) x cross-section of the y-integrated z component of the demagnetizing field, further averaged along a z slice of height 15 nm, calculated around several given z positions from the center of the pillar ($z = 0$). (d) Profile along z of the maximum in absolute value (always found at x=0, *i.e.* on the axis of the pillar) of the curves shown in (c), versus the position of the slice, the latter still with average along z over 15 nm (the color code along z is similar as in (c) for easy understanding).

S2: Quantitative phase calculation

We used 3 different methods for quantifying the spontaneous magnetization in this study. These methods are details hereafter:

Cylinder approximation:

In this first approximation, the nano-pillar is treated as a uniformly-magnetized infinite cylinder of radius *r*. In this case, the magnetic induction transverse to the electron beam direction is only arising from magnetization, and can be calculated using the following equation:

$$\left|\vec{B}\right| = \frac{\hbar \Delta \phi_m}{e\pi r^2} \qquad \text{(S2)}$$

where *e* is the (positive) elementary charge, $\hbar$ is reduced Planck's constant and $\vec{B}$ is the in-plane magnetic induction[3]. Using the measured radius of $r \sim$ 8.6 nm, the value of $\vec{B}$ is calculated as **0.82 ± 0.06 T** with the standard deviation determined from the noise of free space.

Slope measurement and integrated demagnetizing field approximation:

A common method for determining a magnetic flux density from holography phase image is to use a phase profile fitting to extract the integrated flux in a linear part of its plot. The curve of Fig. 2b in the main manuscript has thus been fitted to obtain a slope of 30 ± 2 mrad.nm^{-1}. Such a slope has to be normalized with the Magnetic Flux Quantum

$$\Phi_0 = \frac{e}{2h} = 2.07\ 10^{-15}\text{Wb} = \ 658\ \text{T.nm}^2$$

obtain for the integrated magnetic flux corresponding to the measured phase shift : 19.7 ± 1.4 T.nm. This new estimation should give rise to a value of spontaneous magnetization of 1.14 ± 0.08 T, which does not include the influence of the demagnetizing field that would lower this value. However, such a measurement is a more precise extraction than the previous one which only relies on the overall phase shift, strongly influenced by lateral dipolar field, instead of the phase variation in the vicinity of the pillar.

Due to the finite length of the nano-pillar, it gives rise to a stray field and an internal demagnetizing field from the magnetic charges occurring at both pillar surfaces (see Fig. S1a). These fields contribute to the experimental measurement of the induction, overall opposite to the magnetization direction, so that the above value underestimates the spontaneous magnetization of the material. We thus used Hubert's formalism to compute the integrated

demagnetizing field experienced by the electrons along their trajectory (see Fig. S1(a & d)): 0.72 T.nm is thus found at the middle of the pillar.

We can thus remove the underestimation of the measured integrated magnetic flux corresponding to the magnetization, leading to a final estimation of the spontaneous magnetization of **1.19 ± 0.08 T.** Nevertheless, the estimation of the integrated value of the demagnetizing field suffers from uncertainty as we selected its minimum value. This leads to a substantial underestimation if there is (i) any residual tilt in the experimental projection (S1, parameter 2; and Fig. S1d) or (ii) experimental geometry deviation to the model used that would lead to a displacement of such locale minimum. We eventually applied another correction using experimental estimation of external stray fields using a vectorial field "tomographic" reconstruction in the last section below.

"Tomography" approach:

In order to take into account the influence of the stray field outside the nano-pillar, we reconstructed the 3D magnetic field from a single-phase image using symmetry arguments of the one-dimensional nature of the nano-pillar[4]. The reconstructed 3D field allows isolation of individual planes of magnetic induction through the center of the nanopillar (Fig. S2a) or plane behind the nano-pillar (Fig. S2b). The averaged line profile of $\vec{B}$ acquired from the arrow in Fig. S2a (white) is plotted in Fig. S2c, revealing the large positive value of 1.09 ± 0.01 T from the center of the nano-pillar. Two smaller negative values of 0.075 T are observed on either side of the central peak, and are similar in value to the averaged line profile acquired from the plane behind the nano-pillar (white arrow in Fig. S2b).

Such reconstruction enables the removal of the influence of external stray field on the electron wave as it travels past the nano-pillar. However, we still have to account for the internal demagnetizing field that was computed in previous section. For this, we use the estimation of the demagnetizing field in the vicinity of the pillar (Fig. S1b) which has been estimated at 49mT, leading to a corrected value of the saturated magnetization of **1.14 ± 0.01 T.** This value is in the same range of the one computed with the slope approximation corrected with the integral of the stray field. However, such value is substantially more precise and greater confidence is placed on the stray field calculation, especially considering the geometric approximation for the pillar is only estimated at the right center of the structure.

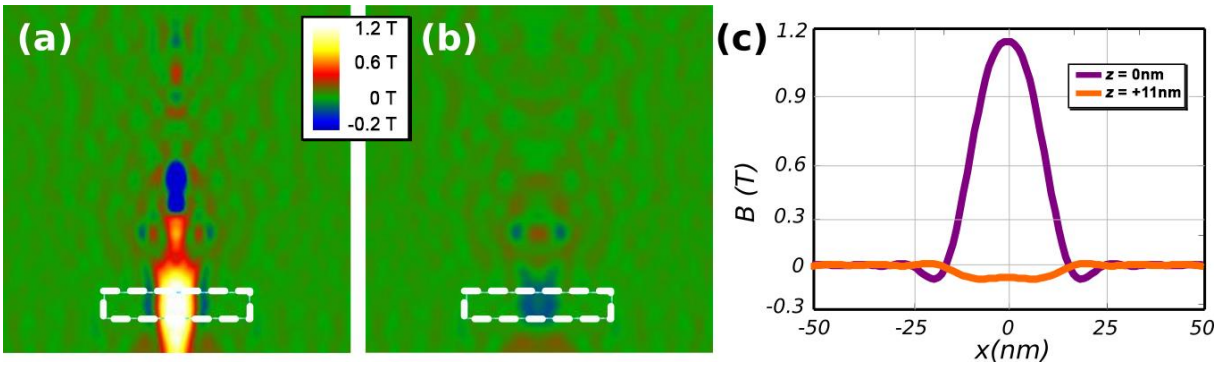

Figure S2. (a,b) Planes of magnetic induction acquired from a 3D reconstruction and measured at the (a) center (0nm); and (b) behind (11 nm) the nano-pillar. (f) Averaged line profiles of magnetic induction measured along the pillar (white dashed area in a & b) comparing the magnetic induction through the center and behind the nano-pillar.

References

1. A. Hubert and R. Schafer, *Magnetic Domains. The Analysis of Magnetic Microstructures*, Springer-Verlag, Berlin, Heidelberg, New York, 1998.
2. R. D. Tikhonov and A. A. Cheremisinov, Magnetization of Permalloy Films, *Russian Microelectronics*, 2017, **46 (2)**, 95–104.
3. K. Chai, Z. Li, W. Huang, G. Richter, R. Liu, B. Zou, J. Caron, A. Kovács, R. E. Dunin-Borkowski and J. Li, Magnetic quantification of single-crystalline Fe and Co nanowires via off-axis electron holography, *J. Chem. Phys.* 2020, **152**, 114202.
4. C. Phatak, L. de Knoop, F. Houdellier, C. Gatel, M. J. Hÿtch and A. Masseboeuf, Quantitative 3D electromagnetic field determination of 1D nanostructures from single projection, *Ultramicroscopy*, 2016, **164**, 24-30.